

Accepted Article

Title: Photo-Responsive Behavior of Azobenzene Based Polar Hockey-Stick-Shaped Liquid Crystals

Authors: Santanu Kumar Pal, Supreet Kaur, Nazma Begum, and Golam Mohiuddin

This manuscript has been accepted after peer review and appears as an Accepted Article online prior to editing, proofing, and formal publication of the final Version of Record (VoR). This work is currently citable by using the Digital Object Identifier (DOI) given below. The VoR will be published online in Early View as soon as possible and may be different to this Accepted Article as a result of editing. Readers should obtain the VoR from the journal website shown below when it is published to ensure accuracy of information. The authors are responsible for the content of this Accepted Article.

To be cited as: *ChemPhysChem* 10.1002/cphc.202100215

Link to VoR: <https://doi.org/10.1002/cphc.202100215>

Photo-Responsive Behavior of Azobenzene Based Polar Hockey-Stick-Shaped Liquid Crystals

Supreet Kaur,^{[a]†} Nazma Begum,^{[a]†} Golam Mohiuddin,^[a] Santanu Kumar Pal^{[a]*}

[a] Ms. S. Kaur,[†] Dr. N. Begum,[†] Dr. G. Mohiuddin, Dr. S. K. Pal*
Department of Chemical Sciences
Indian Institute of Science Education and Research (IISER) Mohali
Sector-81, Knowledge City, Manauli 140306, India.
E-mail: skpal@iisermohali.ac.in

[†] Equally contributed authors.

Supporting information for this article is given via a link at the end of the document.

Abstract: A study on the photoswitching behavior of azobenzene-based polar hockey-stick-shaped liquid crystals (HSLCs) has been presented. Two new series of five phenyl rings based polar HSLCs have been designed and synthesized. Solution state photoisomerization of the synthesized materials was investigated thoroughly via UV-visible and ¹H NMR spectroscopic techniques, whereas solid-state photochromic behavior was elucidated via physical color change of the materials, solid-state UV-visible study, powder XRD, and FE-SEM techniques. The materials exhibited decent photochromic behavior for different potential applications. The thermal phase behavior of the superstructural assembly has been characterized via polarizing optical microscopy (POM), differential scanning calorimetry (DSC), and temperature-dependent small and wide-angle X-ray scattering (SAXS/WAXS) studies. Depending upon the length of the terminal alkyl chain, nematic (N) and partially bilayer smectic A (SmA_d) phases were observed. The DFT calculation revealed the favorable anti-parallel arrangement of the polar molecules that substantiate the formation of SmA_d phase.

Introduction

Photo-responsive functional materials have gained tremendous attention from the scientific community due to their intrinsic physio-chemical behavior and have an immense prospect in device applications.^[1-3] A great deal of effort, in the contemporary era, has been deployed to develop suitable photo-regulated materials or molecular motors. In this context, azobenzene, a versatile photo-functional moiety, has been studied for decades with equal importance as a remarkable photoisomerizable and photochromic unit. Azobenzene exhibits a prominent, facile, and clean geometric change between its *E/Z*- (*trans/cis*) isomers upon irradiation with light, and hence finds potential applications in sensors, actuators, non-linear optic devices, optical data storage, polarization holography, solar energy harvesting, etc.^[4-8] Despite being well-known for over a century, azobenzene-based materials are still being explored in the field of material chemistry,^[9-11] medicinal chemistry,^[12,13] biochemical applications,^[14,15] etc. The molecular structure of liquid crystal (LC) systems incorporated with azobenzene units widens the range of their application due to its photoresponsive behavior.^[16-21] The materials realized from the combination of photosensitivity and LC properties have immense perspective in various optical and optoelectronic devices. In 2001, Prasad et al. reported the first

azobenzene substituted bent-core liquid crystalline materials exhibiting banana-type mesophases.^[22,23] Since then, a library of compounds incorporating five, six, and/or seven aromatic rings in the molecular structure have been prepared to understand the relationship between the structure and the nature of the mesophases.^[24-36] The reports on azobenzene-based bent-core LCs have been reviewed by M. Alaasar.^[37] An interesting photo-orientation phenomenon has been explored in films of azobenzene containing bent-shaped compounds.^[38,39] Owing to the isomerization, light-induced phase transitions i.e. from solid to liquid,^[40-42] and gel to sol^[43] have been enormously discussed in azobenzene based materials. The surface topographies of amorphous, nematic, as well as crystalline films of an azobenzene-containing bent-core compound has been investigated via polarizing optical microscopy and atomic force microscopy.^[44] Recently, we have also reported azobenzene-based four-ring hockey-stick-shaped LCs (HSLCs) and their photoswitching characteristics. The HSLCs with chlorinated (–Cl) azobenzene wings exhibited photo-induced phase transitions in solid-state, LC state, and solution-state upon irradiation with UV as well as intense visible light.^[16] Another class of HSLCs with methylated (–CH₃) azobenzene wings showed a photo masking effect (nematic to isotropic transition) in the LC state upon UV illumination. An optically enhanced Fréedericksz transition has been observed in one of the materials, based on which a prototype of phase grating has been devised for photonic devices.^[17]

Here, we synthesized and investigated two new series of azobenzene-based hockey-stick-shaped compounds comprised of azo-ester-imine-ester linkers (Figure 1). The molecules are terminated with a highly electronegative –NO₂ group at one end and the other end is attached with alkyl chains (n = 4, 6, 8, 12, 18). A methyl (–CH₃) moiety is placed at the lateral positions (X and Y of Figure 1) i.e. on the ring adjacent to the –N=N– linkage.

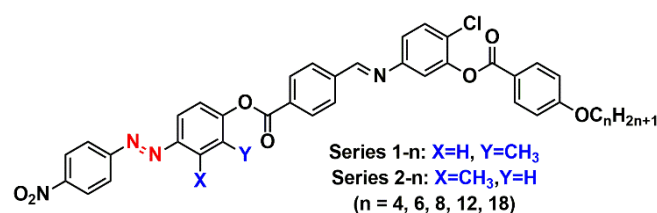
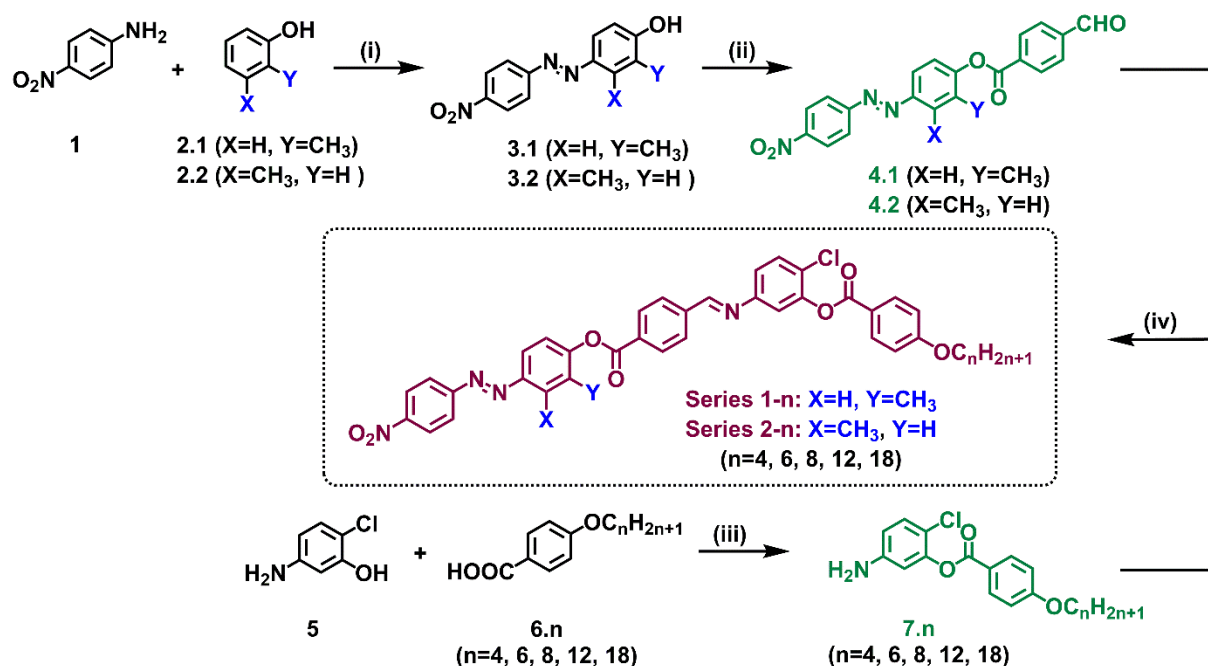


Figure 1. Molecular structure of the hockey-stick-shaped compounds under research.

ARTICLE



Scheme 1. Synthetic scheme of the compounds, Reagents and conditions: (i) HCl, NaNO₂, 0–5 °C, NaOH (75%); (ii) 4-Formylbenzoic acid, DCC, DMAP, Dry CH₂Cl₂, 24 h (85%); (iii) DCC, DMAP, Dry CH₂Cl₂, 24 h (85%); (iv) CH₃OH, CH₂Cl₂, glacial AcOH, reflux, 4h (78%).

By varying the position of –CH₃ group (X and Y) and the terminal flexible alkyl chains, we intend to understand the photoswitching behavior, self-assembly, and materialistic properties of this class of HSLCs.

Results and Discussion

Synthesis and characterization: A general representation of two series (1-n and 2-n) of azo-based hockey-stick-shaped compounds is presented in Figure 1. 5-Amino-2-chlorophenol was taken as the central core to provide the bent-molecular architecture. The desired compounds were synthesized following the schematic procedure as outlined in Scheme 1. All the details of the spectroscopic data, molecular characterization viz. ¹H NMR, ¹³C NMR, HRMS, ATR (Figures S1-S45, Table S1), photoswitching characterization (Figures S46-S49), and material characterization such as POM, DSC, temperature-dependent SAXS/WAXS studies and DFT calculations (Figures S50-S54, Tables S2-S4) are sequentially elaborated in the Supporting Information.

Analysis of photoswitching behavior via UV-visible and NMR techniques: UV-visible spectroscopy is an important technique to understand the *trans-cis* photoisomerization of the azobenzene unit. The spectral features of both *trans* and *cis*-isomers can be well differentiated due to strong changes in the electronic structures. The photoswitching and kinetics studies were carried out in CH₂Cl₂ at room temperature (~ 25 °C). The UV-visible spectrum of compound 1-4 showed a significant absorption maximum (λ_{max}) at 346 nm (10⁻⁴ M, 3.5 eV, ε ~ 10629 L mol⁻¹ cm⁻¹) corresponding to symmetry allowed π-π* transition of the

chromophore (–N=N–) accompanied by a forbidden n-π* transition band at 455 nm as shown in Figure 2a. Upon irradiation with UV light of 365 nm (UV₃₆₅), the intensity of π-π* band decreased (λ ~ 333 nm) whereas the intensity of n-π* band increased (λ ~ 442 nm) indicative of *trans-cis* photoisomerization. A similar trend was observed in the case of compound 2-4 (Figure 2b). The photostationary state (PSS) was found to be 20s and 30s for compounds 1-4 and 2-4, respectively (Figure S46). An additional peak was observed at ~270 nm due to π-π* transition in Schiff's base (–CH=N–) moiety.

To study the effect of positional variance of the methyl group on the stability of the *cis*-isomer, a thermal reverse isomerization kinetics study was carried out using UV-visible spectroscopy (in CH₂Cl₂ at 25±1 °C). Both compounds 1-4 and 2-4 were switched from their respective *trans* to *cis*-isomers using UV₃₆₅ light (i.e. UV light with λ=365 nm) before the thermal reverse isomerization kinetics experiment. The plots of the exponential rate of formation of the *trans*-isomer at an absorbance λ_{max} corresponding to the

Table 1. Absorption spectral properties and formation rate constants in solution phase using UV-visible spectroscopy.

Compound	λ _{max} (ε) (<i>trans</i>)	λ _{π-π*} , λ _{n-π*} (<i>cis</i>)	Rate constant k (10 ⁻³)	Half-life
1-4	346 (10629)	333, 442	9.23	75.05
2-4	351 (9611)	336, 443	3.93	176.34

[The values of λ_{max} (*trans*) and λ_{π-π*}, λ_{n-π*} (*cis*) are given in nm and ε value in L mol⁻¹ cm⁻¹ (in parenthesis). Rate constants (min⁻¹) and the half-lives (min) have been measured in CH₂Cl₂ at 25±1 °C.]

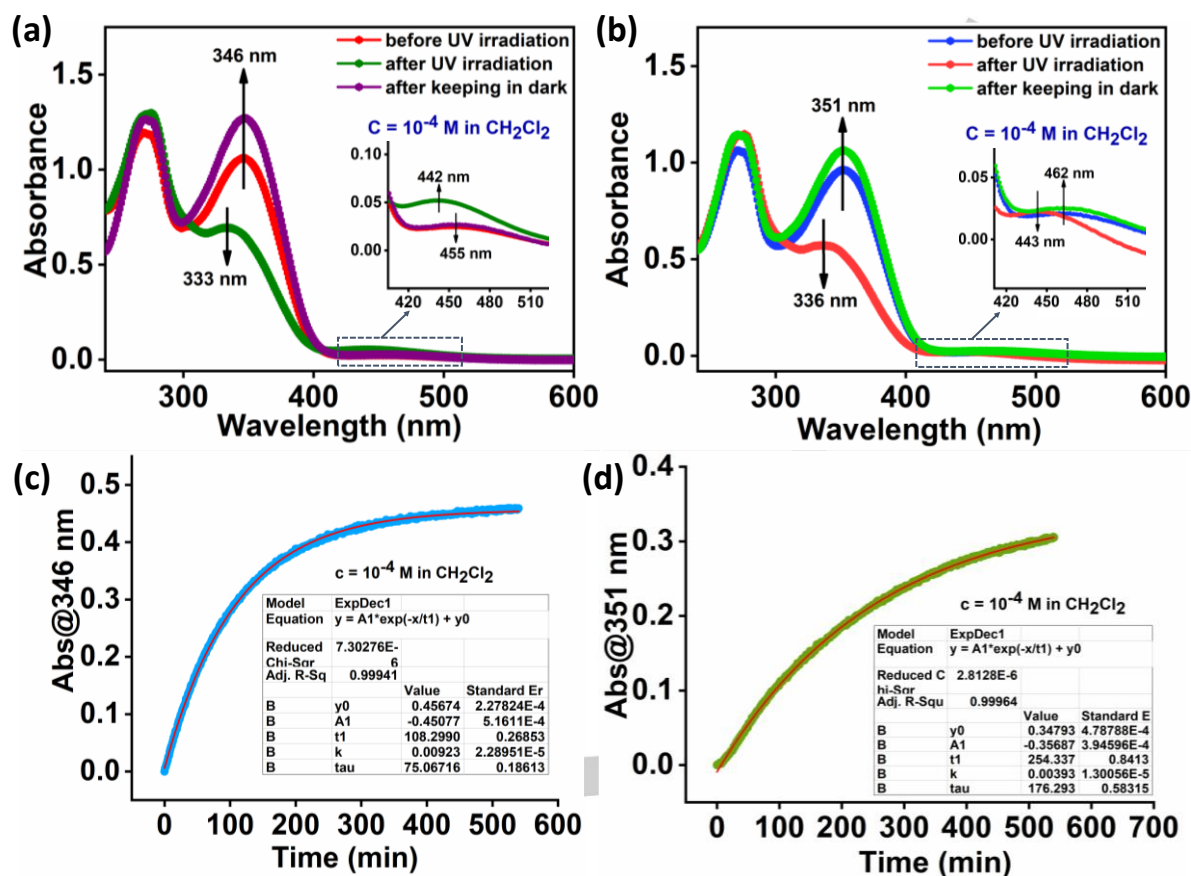


Figure 2. Photoswitching studies of compounds (a) 1-4, (b) 2-4 in CH_2Cl_2 before UV irradiation, after UV irradiation, and after keeping in dark. First-order formation kinetics for the reverse switching (*cis-trans*) in 10^{-4} M solution in CH_2Cl_2 for compounds (c) 1-4 and (d) 2-4.

π - π^* transition of the respective *trans*-isomer ($\lambda_{\text{max}} = 346$ nm and 351 nm for compounds 1-4 and 2-4, respectively) are presented in Figures 2c,d. Following the first-order kinetics, the rate constant, k , and the half-life of the *cis*-isomer were calculated (Table 1). The net rate of formation of the *trans*-isomer of compound 2-4 was observed to be greater than 1-4. The difference in the half-lives and rate constants for both representative compounds arise due to the variation in the lateral substitution of the $-\text{CH}_3$ group adjacent to the $-\text{N}=\text{N}-$ bond.

^1H NMR spectroscopic studies also supported the photoswitching behavior. The photoswitching and reverse thermal isomerization for two representative compounds 1-4 and 2-4 were studied in CDCl_3 at room temperature (25 °C). For compound 2-4, upon UV_{365} light irradiation, an additional significant peak at 8.58 ppm emerged in the upfield region, adjacent to the $-\text{CH}=\text{N}-$ singlet at 8.60 ppm as illustrated in Figure 3b. Upon *trans-cis* isomerization, spectral changes i.e. multiple peaks were observed both in the upfield as well as downfield region (highlighted in grey). Also, a signal at 6.23 ppm appeared after UV exposure (Figure 3b). 27% conversion to *cis*-isomer could be achieved upon UV_{365} exposure for 60 min (7.5 mM) as shown in the zoomed region of Figure 3b. The chemical shift (δ) values did not show any difference before and after UV_{365} light irradiation (Figure 3a,b). The reverse thermal

isomerization (*cis-trans*) was attained after exposure to normal visible light (Figure 3c), and the nature of the peaks obtained was exactly similar to the all *trans*-state spectrum (Figure 3a). Similar results were obtained for compound 1-4 upon UV_{365} exposure (Figure S47). 25% conversion to *cis*-isomer could be achieved upon UV_{365} irradiation for ~120 min. The results for compound 1-4 are elaborated in the Supporting Information. It may be noted that % conversion to *cis*-isomer upon irradiation with UV_{365} was approximately the same for both the representative compounds i.e. 25 % and 27 % for 1-4 and 2-4, respectively for approximately similar UV exposure time.

Solid-state photochromism: Apart from the solution-phase photoswitching (as discussed in the above section), the azobenzene-based compounds were also considered solid-state photochromic materials. A representative compound from both the series (compounds 1-6 and 2-4) was investigated in detail for the photoswitching studies. The compound 1-6 was dissolved in chloroform (CHCl_3) and irradiated with UV_{365} light for ~5 h followed by solvent evaporation and drying under vacuum. A preliminary observation was the color change from yellowish-orange to reddish-orange after UV_{365} light irradiation (Figure 4c). The solid-state photochromism was supported by UV-visible spectroscopic studies in KBr medium. The change in spectral

ARTICLE

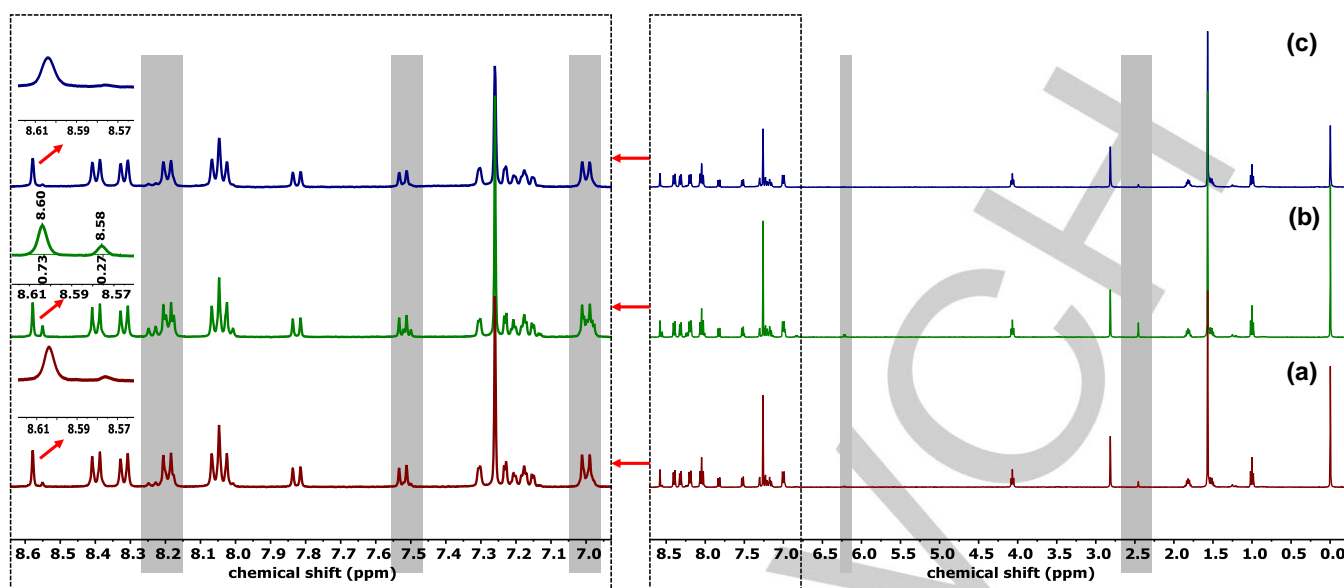


Figure 3. ^1H NMR spectra of compound **2-4** (7.5 mM in CDCl_3): (a) before irradiation, (b) after irradiating with 365 nm UV light for 60 min, (c) after 24 h in normal visible light corresponding to the reverse isomerization. The zoomed regions correspond to the aromatic protons with *trans-cis* conversion, and the changes in the nature and intensity of peaks are highlighted in grey.

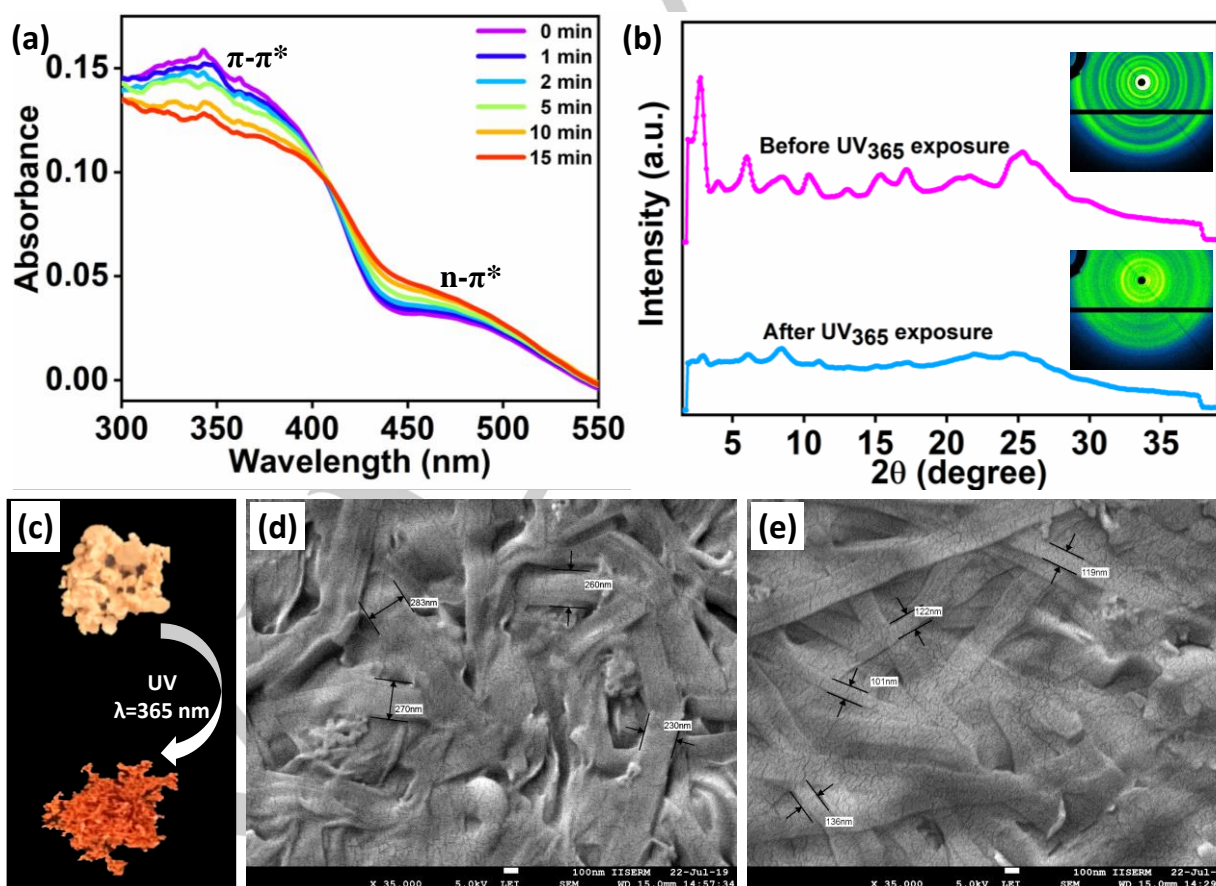


Figure 4. For compound **1-6**: (a) UV-visible spectroscopy in solid-state before (0 min) and after (1, 2, 5, 10, and 15 min) UV_{365} irradiation; (b) X-ray diffraction patterns of the solid sample before (magenta line) and after (blue line) UV irradiation ($\lambda=365$ nm) along with 2D images (inset), at room temperature; (c) photochromism of the solid sample: color switching from yellowish-orange to reddish-orange upon UV_{365} irradiation; FE-SEM images (d) in the pristine state, (e) after irradiation with UV_{365} light (Scale bars: 100 nm, Magnification: X35,000).

ARTICLE

behavior was observed upon UV light irradiation (UV₃₆₅). The comparative intensity of the peak at 346 nm (π - π^* band) decreased whereas the intensity of peak at 465 nm (n - π^* band) increased as UV₃₆₅ was irradiated for 1, 2, 5, 10, 15 min (Figure 4a). The XRD patterns (powder XRD) revealed completely different peaks in the small and the wide-angle region of before (magenta line) and after (blue line) UV light exposed samples (Figure 4b). This experiment confirmed the structural changes in the solid material upon exposure to UV light. The surface morphology of the samples in two states (pristine and after UV irradiation) was studied using FE-SEM (field emission scanning electron microscopy) technique. The SEM micrograph of the pristine sample (before UV) of compound **1-6** showed thick bundles of clumsy and entangled fibers with a diameter in the range of ~230-280 nm (Figure 4d). After UV irradiation, comparatively thin and straight fibers with a reduced diameter of ~100-130 nm (Figure 4e) were observed. The variation in FE-SEM images before and after UV irradiation, is attributed to the structural changes i.e. *trans* and *cis* isomers, respectively. Therefore, photoisomerization of the azobenzene unit reflected in the physical color change, UV-visible spectroscopy, powder XRD and FE-SEM results. Similar experiments were carried out in the case of compound **2-4** to prove the photochromic nature and are detailed in Supporting Information (Figures S48, S49).

Thermal behavior: The thermal behavior of all the compounds was investigated using a combination of polarized optical microscopy (POM) and differential scanning calorimetry (DSC) studies. All the compounds exhibited mesomorphic behavior except **1-4**. The compounds with shorter alkyl chains in both the series ($n = 4, 6, 8$) displayed nematic mesomorphism (**1-4** was non-LC) whereas the ones with longer alkyl chains ($n = 12, 18$) showed SmA phase. The textures were observed under POM with the sample sandwiched between a normal glass slide and coverslip. Upon cooling from the isotropic melt (rate: 5 °C min⁻¹), the compound **2-6** displayed schlieren texture of the nematic phase (Figure 5a) and crystallized at 97.4 °C with a nematic

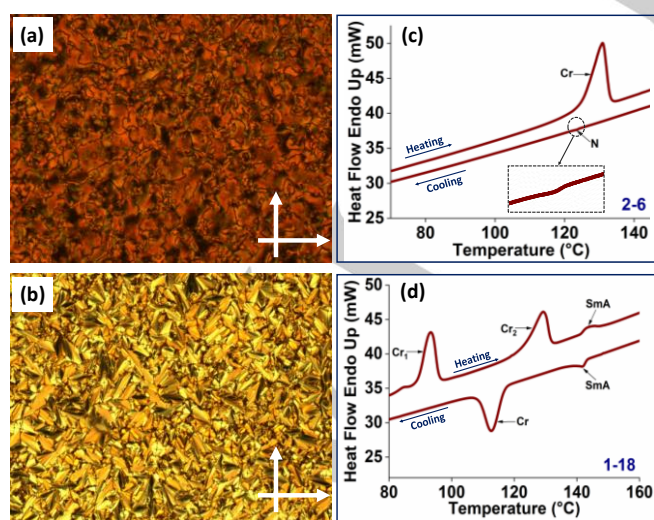


Figure 5. Optical micrographs of two representative compounds on a normal glass slide with coverslip: (a) schlieren texture of the N phase of **2-6** at 123.3 °C and (b) fan-shaped texture of the SmA phase of **1-18** at 126.0 °C (Crossed polarizers, Magnification: X100). DSC thermograms (scan rate: 10 °C min⁻¹) of compounds (c) **2-6** and (d) **1-18**.

Table 2. Thermal properties of the final compounds of series **1-n** and **2-n** recorded from DSC studies (heating and cooling rates: 10 °C min⁻¹).

Compound	Phase transition temperatures in °C (ΔH in kJ mol ⁻¹)
1-4	Heating: Cr 167.7 (45.27) Iso Cooling: Iso 153.0 Cr ^[a]
2-4	Heating: Cr 148.9 (46.62) N 154.1 (0.27) Iso Cooling: Iso 134.8 (-0.02) N 108.3 (-5.85) Cr
1-6	Heating: Cr ₁ 98.1 (-27.96) Cr ₂ 150.6 (25.96) Iso Cooling: Iso 123.8 (-0.04) N 58.2 Cr ^[a]
2-6	Heating: Cr 130.9 (46.80) Iso Cooling: Iso 123.6 (-0.03) N 97.4 Cr ^[a]
1-8	Heating: Cr ^[a] 163.4 N ^[a] 167.0 Iso ^[a] Cooling: Iso ^[a] 128.1 N ^[a] 100.9 Cr ^[a]
2-8	Heating: Cr ^[a] 120.1 N ^[a] 129.5 Iso ^[a] Cooling: Iso ^[a] 130.1 N ^[a] 97.0 Cr ^[a]
1-12	Heating: Cr 127.1 (27.20) SmA 136.0 (1.07) Iso Cooling: Iso 132.7 (-1.25) SmA 92.1 (-16.40) Cr
2-12	Heating: Cr 118.1 (38.43) SmA 128.6 (0.97) Iso Cooling: Iso 123.9 (-0.53) SmA 95.8 (-29.64) Cr
1-18	Heating: Cr ₁ 93.2 (26.53) Cr ₂ 129.1 (23.94) SmA 143.4 (1.88) Iso Cooling: Iso 141.8 °C (-1.59) SmA 112.8 °C (-24.57) Cr
2-18	Heating: Cr ₁ 105.2 (34.77) Cr ₂ 119.2 (32.48) SmA 148.5 (0.64) Iso Cooling: Iso 141.7 (-0.19) SmA 90.6 Cr ^[a]

^[a]Transition temperatures observed from POM and SAXS/WAXS studies.

Abbreviations: Cr = crystal, N = nematic, SmA = smectic A, Iso = isotropic liquid.

phase range of 26.2 °C. Similarly, compound **1-6** also showed an enantiotropic nematic phase (Figure S50b). Homologues with longer alkyl chains, for example, compound **1-18** exhibited focal-conic textures characteristic of the SmA phase (Figure 5b) from 141.8 °C up to crystallization at 112.8 °C and likewise, compound **2-18** displayed SmA phase (Figure S50i). The textures of the remaining mesomorphic compounds are presented in Figure S50 in the Supporting Information. The mesophases observed under POM were further confirmed by SAXS/WAXS studies. The differential scanning calorimetry (DSC) studies provided the phase transition temperatures and the associated enthalpies of all the homologues of series **1-n** and **2-n** as mentioned in Table 2. The DSC spectra of two representative compounds are shown in Figure 5c,d and the rest are presented in the Supporting Information (Figure S51).

Temperature-dependent SAXS/WAXS studies: The intrinsic nature of the self-assembled superstructures of the LC materials was investigated by the temperature-dependent SAXS/WAXS experiments. The XRD profiles of representative compounds from both **1-n** and **2-n** series have been presented in Figure 6. In compound **2-18**, SmA phase was confirmed by the presence of two peaks with layer spacings as $d = 66.40$ Å and $d = 33.22$ Å in the small-angle region at 115 °C (Figure 6a). The wide-angle region showed a diffused halo at $d \sim 4.93$ Å due to the liquid-like correlation of the alkyl chains (Figure S52d). The first and second peaks were assigned reflections of the (100) and (200) planes due

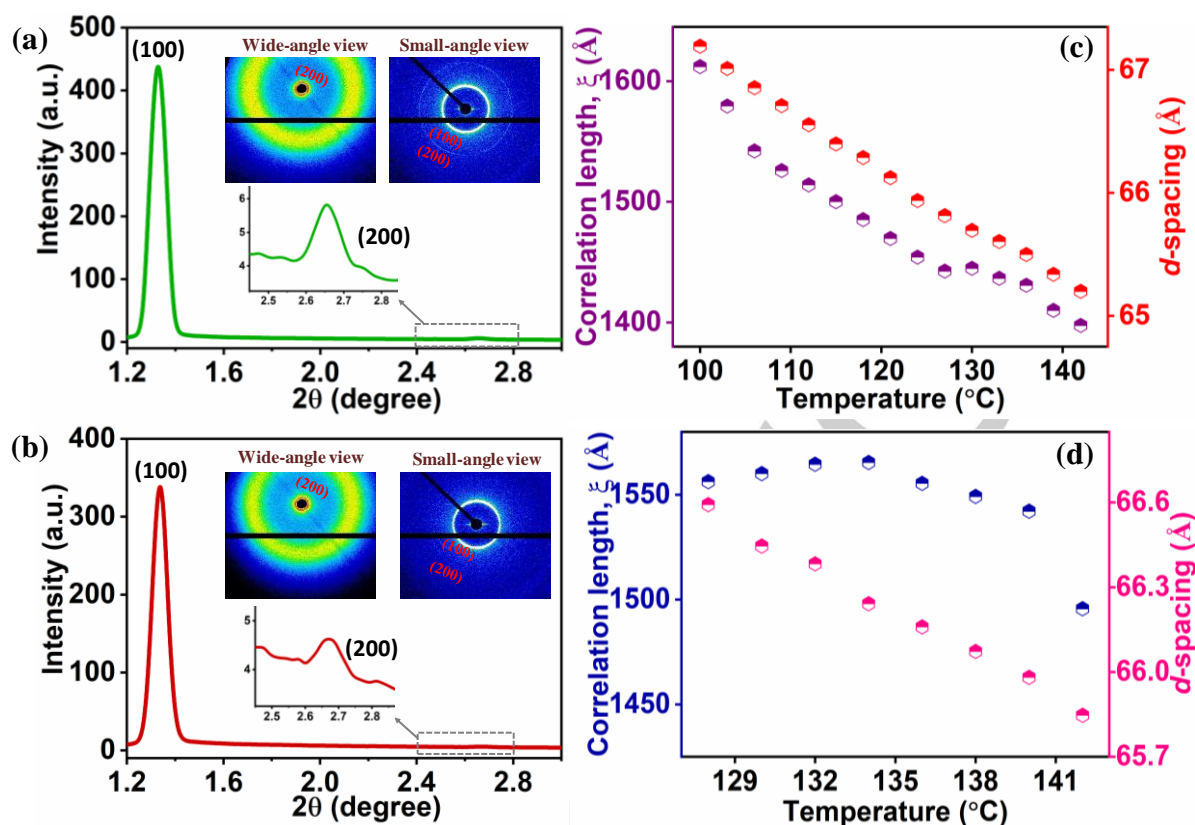


Figure 6. Intensity vs 2θ profile in the SAXS region displaying (100) peak (the (200) peak is zoomed in the inset) along with 2D diffraction images of the small as well as the wide-angle region (inset) in SmA phase of compounds: (a) 2-18 at 115 °C and (b) 1-18 at 140 °C. Variation of correlation length (ξ) and d -spacing corresponding to the first peak (100) as a function of temperature of compounds: (c) 2-18 and (d) 1-18.

to their ratio of layer spacings (66.40/33.22 ~ 2:1). The calculated d/L (where d = layer spacing, L = molecular length from DFT optimized structure) value for compound 2-18 at 115 °C was found to be 1.34 (d = 66.40 Å, L = 49.60 Å; d/L = 1.34 i.e. $d > L$) and indicated the formation of partially bilayer Smectic A phase i.e. SmA_d.^[45] Due to the presence of a polar terminal group, an antiparallel arrangement of the molecules is expected to minimize the overall dipole moment of the bulk material.^[16,17,46,47] The layer spacing d could be assumed as the length of the antiparallel dimeric arrangement of neighboring molecules with overlapping of the rigid cores.^[48] To understand this, we proposed dimers of two representative compounds 1-8 and 2-8 (Figure 7) with the help of Density Functional Theory (DFT) calculations (by employing B3LYP hybrid functional and the 6-311G (d,p) basis set). In the case of compound 1-8, the layer spacing (d ~ 48.36-53.00 Å) calculated from the SAXS/WAXS studies was approximately equivalent to the length of the antiparallel dimeric arrangement of molecules (d ~ 47.28 Å) calculated from the DFT studies. Similar results were observed in compound 2-8 (where d ~ 48.03-53.00 Å from SAXS/WAXS studies and probable d ~ 47.58 Å from DFT studies).

Table 3 represents the calculated binding energy and resultant dipole moment of the respective dimers. There was not much difference observed in the binding energy of both the dimers probably due to the similarity in the composition of the structures. The decrease in the resultant dipole moment of the dimer from its

monomeric form supports the anti-parallel arrangement of the molecules with a highly electronegative $-\text{NO}_2$ end group. Likewise, compound 1-18 displayed three peaks with layer

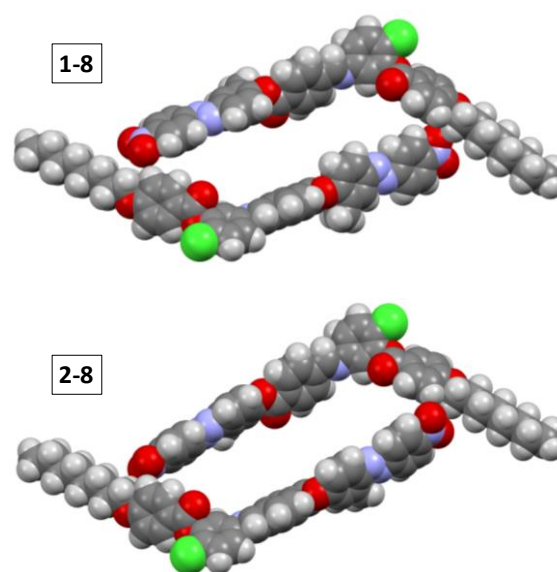


Figure 7. Proposed dimers of compounds 1-8 and 2-8 in a Cartesian coordinate frame, optimized by DFT calculations (B3LYP and 6-311G (d,p)).

ARTICLE

Table 3. The resultant dipole moments of the monomers and the dimers and the binding energy in the dimer form.

Compound	$\mu_{\text{resultant of monomer}}$ (Debye)	$\mu_{\text{resultant of dimer}}$ (Debye)	Binding energy (kJ mol ⁻¹)
1-8	8.02	1.27	34.25
2-8	8.07	0.76	35.07

spacings as $d = 65.98 \text{ \AA}$ (100 peak), $d = 33.06 \text{ \AA}$ (200 peak) and $d = 5.08 \text{ \AA}$ at $140 \text{ }^\circ\text{C}$ (Figure 6b). The d/L was calculated to be 1.34 ($= 65.98/49.40$) and therefore, the phase was designated as partially bilayer Smectic A phase (SmA_d) phase. The temperature-dependent SAXS/WAXS profiles of compound **1-18** are presented in the Supporting Information (Figure S52c). The correlation length (ξ) and d -spacing increased on decreasing the temperature in the entire smectic region for both compounds **2-18** and **1-18** as shown in their respective Figures 6c,d (Table S2 in the Supporting Information). In addition to this, upon lowering the temperature from the isotropic liquid, the intensity of the (100) and (200) peaks in the small-angle region gradually increased throughout the SmA phase range in both compounds **1-18** and **2-18** (Figure S52c,d, respectively).

It was observed that varying the position of the $-\text{CH}_3$ group in the two series did not affect the molecular arrangement i.e. $d \sim 66 \text{ \AA}$ (100 peak) and $d \sim 33 \text{ \AA}$ (200 peak) in the case of both compounds **2-18** and **1-18**. The presence of a highly polar terminal $-\text{NO}_2$ group forced the antiparallel bilayer arrangement in the smectic phase.

The XRD profiles of compounds **1-8** and **2-8** are discussed elaborately in the Supporting Information (Figure S52a,b, Table S2, and Figure S53).

Conclusion

In summary, we have synthesized and investigated two new series of azo-based polar hockey-stick-shaped liquid crystals (HSLCs) and studied their photoswitching behavior in solution as well as in solid-state. UV-visible and ^1H NMR spectroscopic techniques explained the solution state photo-isomerization in the compounds. Solid-state photochromism was observed i.e. color change from yellowish-orange to reddish-orange upon UV light illumination. This observation was well supported by changes in solid-state UV-visible spectroscopy, powder XRD patterns, and FE-SEM images. The optical textures revealed the presence of N and SmA mesophases in the synthesized compounds that was further supported by DSC and temperature-dependent SAXS/WAXS studies. The N phase appeared in the lower homologues ($n = 4, 6, 8$) whereas SmA phase was observed in the higher ones ($n = 12, 18$) of both the series. Overall, the studies reported here would be useful for a general understanding of the photo-isomerization process in azo-based LC materials, and the advancement of molecular design of suitable photo-switching materials for technological applications.

Experimental Section

General

The instrumental details for structural characterization are similar to as mentioned in our previous papers^[46,47,49] and briefed here for the reader's convenience. Structural characterization of the compounds was carried out with a combination of Attenuated total reflectance (ATR; FTIR Bruker-ALPHA Bruker-1227-3513), UV-Vis-NIR spectrophotometer (LABINDIA UV-Vis Spectrophotometer 3000+), High Resolution Mass Spectrometry (Waters synapt g2s), ^1H NMR and ^{13}C NMR (Bruker Biospin Switzerland Avance III 400 MHz and 100 MHz spectrometers, respectively). NMR spectra were recorded using deuterated chloroform (CDCl_3) as solvent and tetramethylsilane (TMS) as an internal standard. FESEM was performed by using a JEOL JSM- 7600F instrument. Polarising Optical Microscopy (POM) textural observations of the mesophases were performed with Nikon Eclipse LV100POL polarising microscope provided with a Linkam heating stage (LTS 420). Differential Scanning Calorimetry (DSC) measurements were performed on Perkin Elmer DSC 8000 coupled to a Controlled Nitrogen Accessory (CLN2) with a scan rate of $10 \text{ }^\circ\text{C min}^{-1}$ both on heating and cooling. X-ray Diffraction (XRD) studies were carried out on samples using $\text{CuK}\alpha$ ($\lambda = 1.54 \text{ \AA}$) radiation from GeniX3D microsource operating at 50kV and 0.6 mA, using Pilatus 200K detector in Xeuss 2.0 SAXS/WAXS system.

General procedure for the synthesis of 1-n and 2-n

The synthetic route for the preparation of the asymmetrical azo-based bent-shaped compounds is presented in Scheme 1 in the manuscript. The final compounds were prepared by performing a Schiff's base reaction. Compound **4.1** or **4.2** (1 eq.) was refluxed in a mixture of methanol:dichloromethane ($\text{CH}_3\text{OH}:\text{CH}_2\text{Cl}_2$:: 50:50) with slow addition of **7.n** (1 eq.) dissolved in CH_3OH with a few drops of glacial acetic acid as catalyst for 4 hours. The crude precipitate was dissolved in hot boiling methanol and the insoluble yellow-orange solid was collected as the pure product. Yield $\sim 78 \%$

Compound 1-4:

^1H NMR (400 MHz, CDCl_3 , δ in ppm): $\delta = 8.59$ (s, 1H, $-\text{CH}=\text{N}-$), 8.40 (d, 2H, $J = 8.0 \text{ Hz}$, Ar-H), 8.35 (d, 2H, $J = 12.0 \text{ Hz}$, Ar-H), 8.20 (d, 2H, $J = 8.0 \text{ Hz}$, Ar-H), 8.08-8.03 (m, 4H, Ar-H), 7.95-7.91 (m, 2H, Ar-H), 7.53 (d, 1H, $J = 8.0 \text{ Hz}$, Ar-H), 7.38 (d, 1H, $J = 8.0 \text{ Hz}$, Ar-H), 7.24 (d, 1H, $J = 4.0 \text{ Hz}$, Ar-H), 7.17 (dd, 1H, $J = 8.0, 4.0 \text{ Hz}$, Ar-H), 7.00 (d, 2H, $J = 8.0 \text{ Hz}$, Ar-H), 4.07 (t, 2H, $J = 8.0 \text{ Hz}$, $-\text{OCH}_2-$), 2.38 (s, 3H, $-\text{CH}_3$), 1.86-1.79 (m, 2H, $-\text{CH}_2-$), 1.54-1.48 (m, 2H, $-\text{CH}_2-$), 1.00 (t, 3H, $J = 8.0 \text{ Hz}$, $-\text{CH}_3$). ^{13}C NMR (100 MHz, CDCl_3 , δ in ppm): $\delta = 13.83, 16.53, 19.20, 31.11, 68.05, 114.42, 116.30, 119.97, 120.61, 122.63, 122.99, 123.44, 124.77, 125.07, 126.03, 129.08, 130.64, 130.69, 131.37, 131.70, 132.57, 140.44, 147.80, 148.69, 150.25, 150.84, 152.56, 155.65, 159.70, 163.87, 163.92, 163.96$. ATR (ν_{max} in cm^{-1}): 1733 ($\nu_{\text{C}=\text{O}}$, ester), 1627 ($\nu_{\text{C}=\text{N}}$, imine), 1608 ($\nu_{\text{C}=\text{C}}$, aromatic), 1525 ($\nu_{\text{N}=\text{O}}$, nitro), 1259 ($\nu_{\text{C}=\text{O}}$, ester), 754 ($\nu_{\text{C}-\text{Cl}}$). HRMS (ESI-MS): m/z calculated for $\text{C}_{38}\text{H}_{32}\text{ClN}_4\text{O}_7$ [$M+\text{H}$]⁺: 691.1959; found: 691.1985.

Compound 1-6:

^1H NMR (400 MHz, CDCl_3 , δ in ppm): $\delta = 8.59$ (s, 1H, $-\text{CH}=\text{N}-$), 8.40 (d, 2H, $J = 8.0 \text{ Hz}$, Ar-H), 8.34 (d, 2H, $J = 8.0 \text{ Hz}$, Ar-H), 8.20 (d, 2H, $J = 8.0 \text{ Hz}$, Ar-H), 8.08-8.03 (m, 4H, Ar-H), 7.95-7.91 (m, 2H, Ar-H), 7.52 (d, 1H, $J = 12.0 \text{ Hz}$, Ar-H), 7.38 (d, 1H, $J = 8.0 \text{ Hz}$, Ar-H), 7.24 (d, 1H, $J = 4.0 \text{ Hz}$, Ar-H), 7.17 (dd, 1H, $J = 8.0, 4.0 \text{ Hz}$, Ar-H), 7.00 (d, 2H, $J = 8.0 \text{ Hz}$, Ar-H), 4.06 (t, 2H, $J = 8.0 \text{ Hz}$, $-\text{OCH}_2-$), 2.38 (s, 3H, $-\text{CH}_3$), 1.87-1.80 (m, 2H, $-\text{CH}_2-$), 1.52-1.45 (m, 2H, $-\text{CH}_2-$), 1.38-1.34 (m, 4H, $-(\text{CH}_2)_2-$), 0.92 (t, 3H, $J = 8.0 \text{ Hz}$, $-\text{CH}_3$). ^{13}C NMR (100 MHz, CDCl_3 , δ in ppm): $\delta = 14.05, 16.53, 22.60, 25.66, 29.04, 31.54, 68.37, 114.43, 116.30, 119.97, 120.60, 122.63, 122.99, 123.44, 124.77, 125.07, 126.03, 129.08, 130.64, 130.69, 131.37, 131.70, 132.57, 140.44, 147.81, 148.69, 150.25, 150.84, 152.56, 155.65, 159.70, 163.87, 163.92, 163.96$. ATR (ν_{max} in cm^{-1}): 2936 ($\nu_{\text{C}-\text{H}}$, alkanes), 1738 ($\nu_{\text{C}=\text{O}}$, ester), 1628 ($\nu_{\text{C}=\text{N}}$, imine), 1609 ($\nu_{\text{C}=\text{C}}$, aromatic), 1528 ($\nu_{\text{N}=\text{O}}$, nitro), 1258 ($\nu_{\text{C}=\text{O}}$, ester), 755 ($\nu_{\text{C}-\text{Cl}}$). HRMS (ESI-MS): m/z calculated for $\text{C}_{40}\text{H}_{36}\text{ClN}_4\text{O}_7$ [$M+\text{H}$]⁺: 719.2272; found: 719.2299.

ARTICLE

Compound 1-8:

¹H NMR (400 MHz, CDCl₃, δ in ppm): δ = 8.59 (s, 1H, -CH=N-), 8.40 (d, 2H, *J* = 8.0 Hz, Ar-H), 8.34 (d, 2H, *J* = 8.0 Hz, Ar-H), 8.20 (d, 2H, *J* = 8.0 Hz, Ar-H), 8.08-8.03 (m, 4H, Ar-H), 7.95-7.91 (m, 2H, Ar-H), 7.52 (d, 1H, *J* = 8.0 Hz, Ar-H), 7.38 (d, 1H, *J* = 8.0 Hz, Ar-H), 7.24 (d, 1H, *J* = 4.0 Hz, Ar-H), 7.17 (d, 1H, *J* = 8.0 Hz, Ar-H), 7.00 (d, 2H, *J* = 8.0 Hz, Ar-H), 4.06 (t, 2H, *J* = 6.0 Hz, -OCH₂-), 2.38 (s, 3H, -CH₃), 1.87-1.80 (m, 2H, -CH₂-), 1.52-1.45 (m, 2H, -CH₂-), 1.40-1.29 (m, 8H, -(CH₂)₄-), 0.90 (t, 3H, *J* = 6.0 Hz, -CH₃). ¹³C NMR (100 MHz, CDCl₃, δ in ppm): δ = 14.12, 16.53, 22.67, 25.98, 29.08, 29.23, 29.33, 31.81, 68.38, 114.43, 116.30, 119.97, 120.60, 122.63, 122.99, 123.44, 124.77, 125.07, 126.03, 129.08, 130.63, 130.69, 131.37, 131.70, 132.57, 140.44, 147.81, 148.69, 150.25, 150.84, 152.56, 155.65, 159.70, 163.87, 163.92, 163.96. ATR (ν_{\max} in cm⁻¹): 2923 (ν_{C-H} , alkanes), 1741, 1730 ($\nu_{C=O}$, ester), 1625 ($\nu_{CH=N}$, imine), 1608 ($\nu_{C=C}$, aromatic), 1526 (ν_{N-O} , nitro), 1262 (ν_{C-O} , ester), 755 (ν_{C-Cl}). HRMS (ESI-MS): *m/z* calculated for C₄₂H₄₀ClN₄O₇ [*M+H*]⁺: 747.2585; found: 747.2554.

Compound 1-12:

¹H NMR (400 MHz, CDCl₃, δ in ppm): δ = 8.59 (s, 1H, -CH=N-), 8.40 (d, 2H, *J* = 8.0 Hz, Ar-H), 8.34 (d, 2H, *J* = 8.0 Hz, Ar-H), 8.20 (d, 2H, *J* = 8.0 Hz, Ar-H), 8.08-8.03 (m, 4H, Ar-H), 7.95-7.91 (m, 2H, Ar-H), 7.52 (d, 1H, *J* = 8.0 Hz, Ar-H), 7.38 (d, 1H, *J* = 8.0 Hz, Ar-H), 7.24 (d, 1H, *J* = 4.0 Hz, Ar-H), 7.17 (dd, 1H, *J* = 8.0, 4.0 Hz, Ar-H), 7.00 (d, 2H, *J* = 8.0 Hz, Ar-H), 4.06 (t, 2H, *J* = 6.0 Hz, -OCH₂-), 2.38 (s, 3H, -CH₃), 1.86-1.79 (m, 2H, -CH₂-), 1.51-1.44 (m, 2H, -CH₂-), 1.39-1.27 (m, 16H, -(CH₂)₈-), 0.88 (t, 3H, *J* = 6.0 Hz, -CH₃). ¹³C NMR (100 MHz, CDCl₃, δ in ppm): δ = 14.13, 16.52, 22.70, 25.99, 29.09, 29.36, 29.57, 29.60, 29.64, 29.66, 31.93, 68.41, 114.46, 116.31, 119.95, 120.65, 122.62, 123.00, 123.44, 124.77, 125.08, 126.05, 129.09, 130.63, 130.69, 131.41, 131.71, 132.57, 140.48, 147.84, 148.74, 150.28, 150.86, 152.59, 155.68, 159.67, 163.89, 163.95. ATR (ν_{\max} in cm⁻¹): 2917 (ν_{C-H} , alkanes), 1736 ($\nu_{C=O}$, ester), 1625 ($\nu_{CH=N}$, imine), 1608 ($\nu_{C=C}$, aromatic), 1528 (ν_{N-O} , nitro), 1260 (ν_{C-O} , ester), 754 (ν_{C-Cl}). HRMS (ESI-MS): *m/z* calculated for C₄₆H₄₈ClN₄O₇ [*M+H*]⁺: 803.3211; found: 803.3231.

Compound 1-18:

¹H NMR (400 MHz, CDCl₃, δ in ppm): δ = 8.59 (s, 1H, -CH=N-), 8.40 (d, 2H, *J* = 8.0 Hz, Ar-H), 8.34 (d, 2H, *J* = 8.0 Hz, Ar-H), 8.20 (d, 2H, *J* = 8.0 Hz, Ar-H), 8.08-8.03 (m, 4H, Ar-H), 7.95-7.91 (m, 2H, Ar-H), 7.52 (d, 1H, *J* = 8.0 Hz, Ar-H), 7.38 (d, 1H, *J* = 8.0 Hz, Ar-H), 7.24 (d, 1H, *J* = 4.0 Hz, Ar-H), 7.17 (d, 1H, *J* = 8.0 Hz, Ar-H), 7.00 (d, 2H, *J* = 8.0 Hz, Ar-H), 4.06 (t, 2H, *J* = 6.0 Hz, -OCH₂-), 2.38 (s, 3H, -CH₃), 1.87-1.79 (m, 2H, -CH₂-), 1.51-1.44 (m, 2H, -CH₂-), 1.36-1.26 (m, 28H, -(CH₂)₁₄-), 0.88 (t, 3H, *J* = 6.0 Hz, -CH₃). ¹³C NMR (100 MHz, CDCl₃, δ in ppm): δ = 14.13, 16.52, 22.70, 25.99, 29.09, 29.37, 29.57, 29.60, 29.67, 29.71, 31.93, 68.40, 114.45, 116.32, 119.95, 120.64, 122.61, 122.99, 123.44, 124.76, 125.07, 126.05, 129.08, 130.63, 130.68, 131.40, 131.70, 132.56, 140.47, 147.83, 148.72, 150.27, 150.85, 152.59, 155.67, 159.67, 163.88, 163.95. ATR (ν_{\max} in cm⁻¹): 2916 (ν_{C-H} , alkanes), 1735 ($\nu_{C=O}$, ester), 1624 ($\nu_{CH=N}$, imine), 1607 ($\nu_{C=C}$, aromatic), 1526 (ν_{N-O} , nitro), 1259 (ν_{C-O} , ester), 755 (ν_{C-Cl}). HRMS (ESI-MS): *m/z* calculated for C₅₂H₆₀ClN₄O₇ [*M+H*]⁺: 887.415; found: 887.4182.

Compound 2-4:

¹H NMR (400 MHz, CDCl₃, δ in ppm): δ = 8.58 (s, 1H, -CH=N-), 8.40 (d, 2H, *J* = 8.0 Hz, Ar-H), 8.32 (d, 2H, *J* = 8.0 Hz, Ar-H), 8.20 (d, 2H, *J* = 12.0 Hz, Ar-H), 8.05 (t, 4H, *J* = 10.0 Hz, Ar-H), 7.83 (d, 1H, *J* = 12.0 Hz, Ar-H), 7.52 (d, 1H, *J* = 8.0 Hz, Ar-H), 7.31 (d, 1H, *J* = 4.0 Hz, Ar-H), 7.24 (d, 1H, *J* = 4.0 Hz, Ar-H), 7.21-7.15 (m, 2H, Ar-H), 7.00 (d, 2H, *J* = 8.0 Hz, Ar-H), 4.07 (t, 2H, *J* = 6.0 Hz, -OCH₂-), 2.81 (s, 3H, -CH₃), 1.86-1.79 (m, 2H, -CH₂-), 1.53-1.50 (m, 2H, -CH₂-), 1.00 (t, 3H, *J* = 8.0 Hz, -CH₃). ¹³C NMR (100 MHz, CDCl₃, δ in ppm): δ = 13.83, 17.72, 19.19, 31.11, 68.05, 114.42, 116.30, 116.91, 119.95, 120.03, 120.61, 123.53, 124.29, 124.77, 125.04, 129.02, 130.62, 130.67, 131.57, 132.56, 140.36, 141.63, 147.80, 148.26, 148.59, 150.85, 153.87, 155.89, 159.74, 163.86, 163.94, 164.23. ATR (ν_{\max} in cm⁻¹): 2968 (ν_{C-H} , alkanes), 1736 ($\nu_{C=O}$, ester), 1627 ($\nu_{CH=N}$, imine),

1611 ($\nu_{C=C}$, aromatic), 1528 (ν_{N-O} , nitro), 1259 (ν_{C-O} , ester), 755 (ν_{C-Cl}). HRMS (ESI-MS): *m/z* calculated for C₃₈H₃₂ClN₄O₇ [*M+H*]⁺: 691.1959; found: 691.1991.

Compound 2-6:

¹H NMR (400 MHz, CDCl₃, δ in ppm): δ = 8.57 (s, 1H, -CH=N-), 8.39 (d, 2H, *J* = 8.0 Hz, Ar-H), 8.31 (d, 2H, *J* = 8.0 Hz, Ar-H), 8.19 (d, 2H, *J* = 8.0 Hz, Ar-H), 8.04 (t, 4H, *J* = 8.0 Hz, Ar-H), 7.82 (d, 1H, *J* = 8.0 Hz, Ar-H), 7.52 (d, 1H, *J* = 8.0 Hz, Ar-H), 7.30 (d, 1H, *J* = 2.5 Hz, Ar-H), 7.23 (d, 1H, *J* = 2.2 Hz, Ar-H), 7.14-7.20 (m, 2H, Ar-H), 7.00 (d, 2H, *J* = 12.0 Hz, Ar-H), 4.05 (t, 2H, *J* = 6.0 Hz, -OCH₂-), 2.81 (s, 3H, -CH₃), 1.86-1.79 (m, 2H, -CH₂-), 1.52-1.45 (m, 2H, -CH₂-), 1.38-1.33 (m, 4H, -(CH₂)₂-), 0.92 (t, 3H, *J* = 8.0 Hz, -CH₃). ¹³C NMR (100 MHz, CDCl₃, δ in ppm): δ = 14.03, 17.71, 22.59, 25.66, 29.05, 31.54, 68.39, 114.44, 116.31, 116.94, 119.93, 120.02, 120.65, 123.52, 124.28, 124.77, 125.05, 129.02, 130.62, 130.66, 131.59, 132.56, 140.39, 141.61, 147.83, 148.28, 148.62, 150.86, 153.90, 155.92, 159.72, 163.87, 163.94, 164.22. ATR (ν_{\max} in cm⁻¹): 2934 (ν_{C-H} , alkanes), 1735 ($\nu_{C=O}$, ester), 1624 ($\nu_{CH=N}$, imine), 1611 ($\nu_{C=C}$, aromatic), 1528 (ν_{N-O} , nitro), 1257 (ν_{C-O} , ester), 754 (ν_{C-Cl}). HRMS (ESI-MS): *m/z* calculated for C₄₀H₃₆ClN₄O₇ [*M+H*]⁺: 719.2272; found: 719.2242.

Compound 2-8:

¹H NMR (400 MHz, CDCl₃, δ in ppm): δ = 8.57 (s, 1H, -CH=N-), 8.39 (d, 2H, *J* = 8.0 Hz, Ar-H), 8.31 (d, 2H, *J* = 8.0 Hz, Ar-H), 8.19 (d, 2H, *J* = 8.0 Hz, Ar-H), 8.04 (t, 4H, *J* = 8.0 Hz, Ar-H), 7.82 (d, 1H, *J* = 8.0 Hz, Ar-H), 7.52 (d, 1H, *J* = 8.0 Hz, Ar-H), 7.30 (d, 1H, *J* = 1.2 Hz, Ar-H), 7.23 (d, 1H, *J* = 2.4 Hz, Ar-H), 7.20-7.14 (m, 2H, Ar-H), 7.00 (d, 2H, *J* = 8.0 Hz, Ar-H), 4.06 (t, 2H, *J* = 6.0 Hz, -OCH₂-), 2.81 (s, 3H, -CH₃), 1.86-1.79 (m, 2H, -CH₂-), 1.52-1.44 (m, 2H, -CH₂-), 1.39-1.29 (m, 8H, -(CH₂)₄-), 0.90 (t, 3H, *J* = 6.0 Hz, -CH₃). ¹³C NMR (100 MHz, CDCl₃, δ in ppm): δ = 14.12, 17.72, 22.67, 25.98, 29.08, 29.23, 29.32, 31.81, 68.37, 114.42, 116.30, 116.91, 119.95, 120.03, 120.59, 123.53, 124.28, 124.77, 125.04, 129.02, 130.62, 130.66, 131.56, 132.56, 140.36, 141.63, 147.80, 148.25, 148.59, 150.84, 153.87, 155.88, 159.74, 163.86, 163.95, 164.23. ATR (ν_{\max} in cm⁻¹): 2923 (ν_{C-H} , alkanes), 1734 ($\nu_{C=O}$, ester), 1623 ($\nu_{CH=N}$, imine), 1607 ($\nu_{C=C}$, aromatic), 1529 (ν_{N-O} , nitro), 1256 (ν_{C-O} , ester), 755 (ν_{C-Cl}). HRMS (ESI-MS): *m/z* calculated for C₄₂H₄₀ClN₄O₇ [*M+H*]⁺: 747.2585; found: 747.2612.

Compound 2-12:

¹H NMR (400 MHz, CDCl₃, δ in ppm): δ = 8.58 (s, 1H, -CH=N-), 8.40 (d, 2H, *J* = 8.0 Hz, Ar-H), 8.32 (d, 2H, *J* = 8.0 Hz, Ar-H), 8.20 (d, 2H, *J* = 12.0 Hz, Ar-H), 8.05 (t, 4H, *J* = 10.0 Hz, Ar-H), 7.83 (d, 1H, *J* = 12.0 Hz, Ar-H), 7.52 (d, 1H, *J* = 8.0 Hz, Ar-H), 7.31 (d, 1H, *J* = 4.0 Hz, Ar-H), 7.23 (d, 1H, *J* = 2.4 Hz, Ar-H), 7.21-7.15 (m, 2H, Ar-H), 7.00 (d, 2H, *J* = 8.0 Hz, Ar-H), 4.06 (t, 2H, *J* = 6.0 Hz, -OCH₂-), 2.81 (s, 3H, -CH₃), 1.86-1.79 (m, 2H, -CH₂-), 1.51-1.44 (m, 2H, -CH₂-), 1.39-1.27 (m, 16H, -(CH₂)₈-), 0.88 (t, 3H, *J* = 6.0 Hz, -CH₃). ¹³C NMR (100 MHz, CDCl₃, δ in ppm): δ = 14.17, 17.75, 22.73, 26.00, 29.10, 29.39, 29.59, 29.62, 29.67, 29.69, 31.95, 68.41, 114.46, 116.35, 116.94, 119.99, 120.05, 120.63, 123.56, 124.31, 124.80, 125.07, 129.05, 130.65, 130.69, 131.59, 132.59, 140.39, 141.66, 147.83, 148.28, 148.62, 150.87, 153.91, 155.92, 159.78, 163.89, 163.98, 164.26. ATR (ν_{\max} in cm⁻¹): 2917 (ν_{C-H} , alkanes), 1748, 1736 ($\nu_{C=O}$, ester), 1624 ($\nu_{CH=N}$, imine), 1609 ($\nu_{C=C}$, aromatic), 1530 (ν_{N-O} , nitro), 1258 (ν_{C-O} , ester), 755 (ν_{C-Cl}). HRMS (ESI-MS): *m/z* calculated for C₄₆H₄₈ClN₄O₇ [*M+H*]⁺: 803.3211; found: 803.3246.

Compound 2-18:

¹H NMR (400 MHz, CDCl₃, δ in ppm): δ = 8.58 (s, 1H, -CH=N-), 8.40 (d, 2H, *J* = 8.0 Hz, Ar-H), 8.32 (d, 2H, *J* = 8.0 Hz, Ar-H), 8.20 (d, 2H, *J* = 12.0 Hz, Ar-H), 8.05 (t, 4H, *J* = 10.0 Hz, Ar-H), 7.83 (d, 1H, *J* = 8.0 Hz, Ar-H), 7.52 (d, 1H, *J* = 8.0 Hz, Ar-H), 7.31 (d, 1H, *J* = 4.0 Hz, Ar-H), 7.23 (d, 1H, *J* = 2.4 Hz, Ar-H), 7.21-7.15 (m, 2H, Ar-H), 7.00 (d, 2H, *J* = 8.0 Hz, Ar-H), 4.06 (t, 2H, *J* = 6.0 Hz, -OCH₂-), 2.81 (s, 3H, -CH₃), 1.86-1.79 (m, 2H, -

ARTICLE

CH₂-), 1.51-1.44 (m, 2H, -CH₂-), 1.39-1.26 (m, 28H, -(CH₂)₁₄-), 0.88 (t, 3H, *J* = 6.0 Hz, -CH₃). ¹³C NMR (100 MHz, CDCl₃, δ in ppm): δ = 14.13, 17.71, 22.70, 25.99, 29.09, 29.37, 29.57, 29.60, 29.67, 29.71, 31.93, 68.39, 114.44, 116.32, 116.93, 119.93, 120.02, 120.64, 123.52, 124.27, 124.76, 125.05, 129.02, 129.70, 130.62, 130.66, 130.83, 131.59, 132.56, 140.38, 141.61, 147.82, 148.27, 148.62, 150.85, 153.90, 155.91, 159.71, 163.87, 163.93, 164.21. ATR (*v*_{max} in cm⁻¹): 2934 (*v*_{C-H}, alkanes), 1735 (*v*_{C=O}, ester), 1624 (*v*_{CH=N}, imine), 1611 (*v*_{C=C}, aromatic), 1528 (*v*_{N-O}, nitro), 1257 (*v*_{C-O}, ester), 754 (*v*_{C-Cl}). HRMS (ESI-MS): *m/z* calculated for C₅₂H₆₀ClN₄O₇ [*M*+H]⁺: 887.415; found: 887.4191.

Acknowledgements

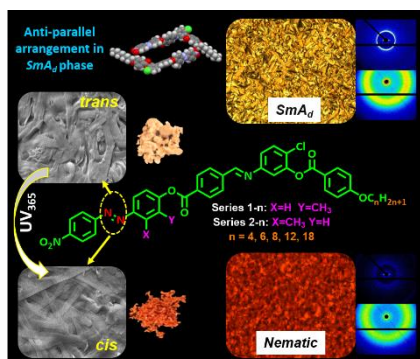
SKP acknowledges SERB Project (CRG/2019/000901/OC). SK acknowledges CSIR (09/947(0254)/2020-EMR-I) and IISER Mohali for PhD fellowship. N.B. acknowledges DST, India for the Women Scientist-A (SR-WOS-A-CS-26-2017) award. GM acknowledges DST-SERB, India for NPDF (NPDF/2016/000560). We thank IISER Mohali for all central, departmental facilities, in particular, for access to the NMR, HRMS, FESEM, and SAXS/WAXS system.

Keywords: Azobenzene • hockey-stick-shaped liquid crystals • Polar liquid crystals • Photo-isomerization • X-ray diffraction

- [1] H. K. Bisoyi, Q. Li, *Chem. Rev.* **2016**, *116*, 15089-15166.
- [2] C. Brieke, F. Rohrbach, A. Gottschalk, G. Mayer, A. Heckel, *Angew. Chem., Int. Ed.* **2012**, *51*, 8446-8476.
- [3] H. Jing, M. Xu, Y. Xiang, E. Wang, D. Liu, A. Poryvai, M. Kohout, N. Éber, Á. Buka, *Adv. Opt. Mater.* **2019**, *7*, 1801790.
- [4] X. Zhou, T. Zifer, B. M. Wong, K. L. Krafcik, F. Leonard, A. L. Vance, *Nano Lett.* **2009**, *9*, 1028-1033.
- [5] Y. Yu, M. Nakano, T. Ikeda, *Nature* **2003**, *425*, 145.
- [6] N. Hosono, T. Kajitani, T. Fukushima, K. Ito, S. Sasaki, M. Takata, T. Aida, *Science* **2010**, *330*, 808-811.
- [7] J. A. Delaire, K. Nakatani, *Chem. Rev.* **2000**, *100*, 1817-1846.
- [8] A. S. Matharu, S. Jeeva, P. S. Ramanujam, *Chem. Soc. Rev.* **2007**, *36*, 1868-1880.
- [9] J. Ge, Y. Yin, *Angew. Chem., Int. Ed.* **2011**, *50*, 1492-1522.
- [10] S. Guo, K. Matsukawa, T. Miyata, T. Okubo, K. Kuroda, A. Shimojima, *J. Am. Chem. Soc.* **2015**, *137*, 15434-15440.
- [11] S. Kobatake, S. Takami, H. Muto, T. Ishikawa, M. Irie, *Nature* **2007**, *446*, 778-781.
- [12] M. M. Lerch, M. J. Hansen, G. M. van Dam, W. Szymanski, B. L. Feringa, *Angew. Chem. Int. Ed.* **2016**, *55*, 10978-10999.
- [13] J. Broichhagen, J. A. Frank, N. R. Johnston, R. K. Mitchell, K. Smid, P. Marchetti, M. Bugliani, G. A. Rutter, D. Trauner, D. J. Hodson, *Chem. Commun.* **2015**, *51*, 6018-6021.
- [14] A. A. Beharry, G. A. Woolley, *Chem. Soc. Rev.* **2011**, *40*, 4422-4437.
- [15] R. J. Mart, R. K. Allemann, *Chem. Commun.* **2016**, *52*, 12262-12277.
- [16] N. Begum, S. Kaur, G. Mohiuddin, R. Nandi, S. P. Gupta, N. V. S. Rao, S. K. Pal, *J. Phys. Chem. B* **2019**, *123*, 4443-4451.
- [17] N. Begum, S. Kaur, Y. Xiang, H. Yin, G. Mohiuddin, N. V. S. Rao, S. K. Pal, *J. Phys. Chem. C* **2020**, *124*, 874-885.
- [18] M. K. Paul, S. K. Saha, G. Kalita, B. Bhattacharya, U. Sarkar, *Dyes and Pigments* **2020**, *173*, 107233.
- [19] M. V. Srinivasan, P. Kannan, A. Roy, *New J. Chem.* **2013**, *37*, 1584-1590.
- [20] N. G. Nagaveni, A. Roy, V. Prasad, *J. Mater. Chem.* **2012**, *22*, 8948-8959.
- [21] N. Trišović, J. Antanasijević, T. T. Katona, M. Kohout, M. Salamonczyk, S. Sprunt, A. Jákli, K. F. Csorba, *RSC Adv.* **2015**, *5*, 64886-64891.
- [22] V. Prasad, D. S. S. Rao, S. K. Prasad, *Liq. Cryst.* **2001**, *28*, 643-646.
- [23] V. Prasad, *Mol. Cryst. Liq. Cryst.* **2000**, *363*, 167-179.
- [24] M. K. Paul, G. Kalita, A. R. Laskar, S. Debnath, V. Gude, D. D. Sarkar, G. Mohiuddin, S. K. Varshney, N. V. S. Rao, *J. Mol. Struct.* **2013**, *1049*, 78-89.
- [25] K. Upadhyaya, V. Gude, G. Mohiuddin, N. V. S. Rao, *Beilstein J. Org. Chem.* **2013**, *9*, 26-35.
- [26] D. D. Sarkar, R. Deb, N. Chakraborty, N. V. S. Rao, *Liq. Cryst.* **2012**, *39*, 1003-1010.
- [27] V. Gude, K. Upadhyaya, G. Mohiuddin, N. V. S. Rao, *Liq. Cryst.* **2013**, *40*, 120-129.
- [28] M. Alaasar, M. Prehm, C. Tschierske, *Liq. Cryst.* **2014**, *41*, 126-136.
- [29] M. Alaasar, S. Poppe, C. Tschierske, *Liq. Cryst.* **2017**, *44*, 729-737.
- [30] N. Sebastián, S. Belau, A. Eremin, M. Alaasar, M. Prehm, C. Tschierske, *Phys. Chem. Chem. Phys.* **2017**, *19*, 5895-5905.
- [31] M. Alaasar, M. Prehm, C. Tschierske, *Chem. Eur. J.* **2016**, *22*, 6583-6597.
- [32] M. Alaasar, M. Prehm, C. Tschierske, *RSC Adv.* **2016**, *6*, 82890-82899.
- [33] M. Alaasar, M. Prehm, M. Brautzsch, C. Tschierske, *Soft Matter* **2014**, *10*, 7285-7296.
- [34] M. Alaasar, M. Prehm, C. Tschierske, *Chem. Commun.* **2013**, *49*, 11062-11064.
- [35] M. Alaasar, M. Prehm, S. Poppe, C. Tschierske, *Chem. Eur. J.* **2017**, *23*, 5541-5556.
- [36] M. Alaasar, M. Prehm, M. Brautzsch, C. Tschierske, *J. Mater. Chem. C* **2014**, *2*, 5487-5501.
- [37] M. Alaasar, *Liq. Cryst.* **2016**, *43*, 2208-2243.
- [38] M. G. Tamba, A. Bobrovsky, V. Shibaev, G. Pelzl, U. Baumeister, W. Weissflog, *Liq. Cryst.* **2011**, *38*, 1531-1550.
- [39] A. Bobrovsky, V. Shibaev, V. Hamplová, A. Bubnov, V. Novotna, M. Kašpar, A. Piryazev, D. Anokhin, D. Ivanov, *J. Photochem. Photobiol. A: Chemistry* **2016**, *316*, 75-87.
- [40] W. C. Xu, S. Sun, S. Wu, *Angew. Chem. Int. Ed.* **2019**, *58*, 9712-9740.
- [41] A. S. Kuenstler, K. D. Clark, J. R. de Alaniz, R. C. Hayward, *ACS Macro Lett.* **2020**, *9*, 902-909.
- [42] S. Ito, A. Yamashita, H. Akiyama, H. Kihara, M. Yoshida, *Macromolecules* **2018**, *51*, 3243-3253.
- [43] A. Bobrovsky, V. Shibaev, V. Hamplová, V. Novotna, M. Kašpar, *RSC Adv.* **2015**, *5*, 56891-56895.
- [44] A. Bobrovsky, K. Mochalov, V. Oleinikov, D. Solovyeva, V. Shibaev, Y. Bogdanova, V. Hamplová, M. Kašpar, A. Bubnov, *J. Phys. Chem. B* **2016**, *120*, 5073-5082.
- [45] R. Dabrowski, *Liq. Cryst.* **2015**, *42*, 783-818.
- [46] S. Kaur, V. Punjani, G. Mohiuddin, S. K. Pal, *New J. Chem.* **2017**, *41*, 5403-5411.
- [47] S. Kaur, G. Mohiuddin, V. Punjani, R. K. Khan, S. Ghosh, S. K. Pal, *J. Mol. Liq.* **2019**, *295*, 111687.
- [48] A. J. Leadbetter, J. C. Frost, J. P. Gaughan, G. W. Gray, A. Mosley, *J. Phys. France* **1979**, *40*, 375-380.
- [49] S. Kaur, G. Mohiuddin, P. Satapathy, R. Nandi, V. Punjani, S. K. Prasad, S. K. Pal, *Mol. Syst. Des. Eng.* **2018**, *3*, 839-852.

ARTICLE

Entry for the Table of Contents



New Azobenzene based polar hockey-stick-shaped liquid crystals displaying photo-switching behavior